Focusing of Optical Vector-vortex Beams

Geo M. Philip[1] and Nirmal K. Viswanathan[1*]

[1]*School of Physics, University of Hyderabad, Hyderabad 500046, India.*

Authors' contributions

The first author GMP was carried out all the calculations, simulations and experiments under the supervision of the second author NKV. The draft versions of the manuscript were written by the author GMP and corrected by the author NKV. Both authors have read and approved final manuscript.

Original Research Article

ABSTRACT

Theoretical formalism using vectorial Rayleigh diffraction integrals is developed to calculate the electric field components (E_x, E_y, E_z) of generalized vector-vortex (VV) beams of different phase and polarization characteristics as a function of propagation distance 'z' in the focal region of an axicon. This formalism is used to generate sub-wavelength spot-size (0.43λ) ultra-long length (80λ) longitudinally-polarized optical needle beam by appropriately selecting the phase and polarization characteristics of the input VV beam. The formalism is further extended to also generate purely transverse polarized beam with similar characteristics. The focusing process leads to interference between different field components of the beam resulting in the formation of *C*-point polarization singularities of index I_c = ±1 whose transverse characteristics evolve with propagation distance. Experimental results to support our theoretical calculations are presented along with lens focus comparison results.

1. INTRODUCTION

Optical beams with spatially varying state of polarization with cylindrical symmetry are known as cylindrical vector beams [1]. As the focusing characteristics of optical beams strongly

---

*Corresponding author: E-mail: nirmalsp@uohyd.ernet.in;

depend on the state of polarization, especially in the non-paraxial regime, the high numerical aperture (NA) focusing of vector beams results in unusual electric field distributions in the focal region [1]. For a generalized vector beam the electric field vector makes a fixed angle of δ with the radial direction [1] with δ =0º for radially polarized vector beam and δ =90º for azimuthally polarized vector beam. The focusing properties of radial and azimuthal polarized vector beams using high NA lenses are well studied both experimentally and theoretically [2-4]. Optical vector beam with suitably engineered polarization and phase structures can give rise to sub-wavelength spot-size non-diverging beams on high-NA focusing [5,6]. These non-diverging vector beams are widely used in super resolution microscopy [7], laser focusing acceleration of electrons [8] and optical tweezers [9].

In addition to the spatially varying polarization the optical vector beam can also carry helical phase structure making it a vector-vortex (VV) beam. It was shown recently that focusing of annular radially polarized beam can give much smaller spot sizes [10], leading to the possibility of encoding phase structure on to vector beams to generate smaller spot sizes [6].Focusing of VV beams can generate transversely-polarized non-diffracting beams [11]. The reduction of spot size happens at the expense of depth of focus (DOF), the sharper the focusing smaller will be the DOF. But extended DOF is needed in many applications including optical imaging. Though there are methods such as wave-front coding [12], annular illumination [13] and adaptive optics techniques [14] available to extend the focal region, the axicon lens [15] based method is one of the simple ones. Most of the studies using axicon for imaging and formation of non-diverging Bessel-Gauss beams are restricted to the scalar regime. In this work we present the axicon focusing characteristics for vector-vortex input beams, extending the usefulness of the treatment to complex phase and polarization engineered optical beam focusing. Toward this we first develop the theoretical formalism based on vectorial Rayleigh diffracting integrals to explain the focusing characteristics of generalized VV beam by an axicon.

Vector beams are also known to possess V-singularity in the beam cross section where the orientation of the linear polarization is not defined [16]. Superposition of orthogonal circularly polarized plane wave and phase dislocated beams can lead to the formation of C and L singularities where the orientation of the major axis and ellipticity of the polarization ellipse respectively are not defined [16,17]. Though it is known that high-NA focusing of azimuthally [18] and radially [19] polarized beams lead to the generation of polarization singular (PS) beams, experimental realization of the PS patterns are difficult since the focal region in high NA focus is very small (few multiples of λ). Axicon focusing enables us to experimentally measure the PS pattern and its evolution due to the extended focal region. By solving the vectorial diffraction integrals for the focusing of generalized VV beam we explain the fine structure of field and the evolution of optical field in the focal region. The interesting aspects of axicon focusing of VV beams is to realize optical beams with purely transverse and longitudinal non-diverging beams which are explained using the developed theoretical formalism.

2. VECTOR DIFFRACTION THEORY

We use vectorial Rayleigh diffraction integrals to calculate the (x, y, z) components of the electric field vector of a vector-vortex beam focused by an axicon at any position along the axis. The schematic of the focusing system that is useful to understand the formalism is shown in Fig.1. An inhomogeneously polarized (vectorial) optical beam with a phase vortex at its center, the vector-vortex (VV) beam is focused by an axicon (A) of open angle 'α'. The

input beam with such phase and polarization characteristics can be generated by passing a generalized cylindrical vector beam (CVB) through a spiral phase plate (SPP). Vectorial Rayleigh diffraction integral is used to calculate the electric field of the monochromatic electromagnetic wave at any point $E(r)$ in the beam cross section propagating in a homogeneous medium by knowing the field distribution at the input z=0 plane [20,21].
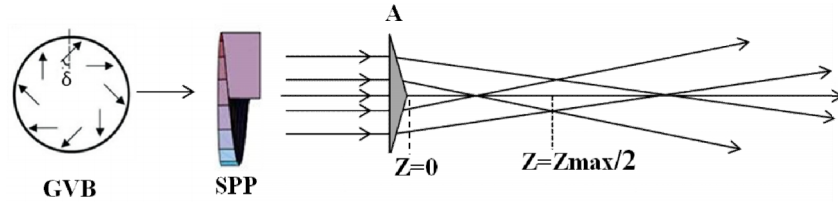

Fig. 1. Schematic of the focusing system, GVB-generalized vector beam, SPP-spiral phase plate, A-axicon, Zmax/2-centre of the non-diverging region

The electric field components are written using the Rayleigh diffraction integral in cylindrical coordinate system as [22]

$$E_x(\rho,\beta,z) = \frac{-iz\exp(ikr)}{\lambda r^2}\int_0^\infty d\rho_0 \int_0^{2\pi} d\phi E_x(r_0) \times \exp(ik\frac{\rho_0^2}{2r})\exp[\frac{-ik\rho\rho_0 cos(\phi-\beta)}{r}]\rho_0 \tag{1a}$$

$$E_y(\rho,\beta,z) = \frac{-iz\exp(ikr)}{\lambda r^2}\int_0^\infty d\rho_0 \int_0^{2\pi} d\phi E_y(r_0) \times \exp(ik\frac{\rho_0^2}{2r})\exp[\frac{-ik\rho\rho_0 cos(\phi-\beta)}{r}]\rho_0 \tag{1b}$$

$$E_z(\rho,\beta,z) = \frac{-i\exp(ikr)}{\lambda r^2}\int_0^\infty d\rho_0 \int_0^{2\pi} d\phi [E_x(r_0)(\rho cos\beta - \rho_0\cos\phi) + E_y(r_0)(\rho\sin\beta - \rho_0\sin\phi)] \times$$

$$\exp(ik\frac{\rho_0^2}{2r})\exp[\frac{-ik\rho\rho_0 cos(\phi-\beta)}{r}]\rho_0 \tag{1c}$$

Where, (ρ,β,z) are the cylindrical coordinates at the observation point and (ρ_0,ϕ) the polar coordinates of the plane immediately after the focusing axicon. Taking into consideration the polarization aspects, the electric field of the input beam to the axicon can be written as

$$E(r_0) = \begin{pmatrix} E_x(r_0) \\ E_y(r_0) \\ E_z(r_0) \end{pmatrix} = P(\theta,\phi)A(\rho_0,\phi) \tag{2}$$

Where $P(\theta,\phi)$ is the polarization matrix and $A(\rho_0,\phi)$ is the amplitude and phase distribution of electric field after the axicon. The polarization matrix for the axicon is [23]

$$P(\theta,\phi) = \begin{pmatrix} 1+\cos^2\phi(\cos\theta-1) & \sin\phi\cos\phi(\cos\theta-1) & \cos\phi\sin\theta \\ \sin\phi\cos\phi(\cos\theta-1) & 1+\sin^2\phi(\cos\theta-1) & \sin\phi\sin\theta \\ -\sin\theta\cos\phi & -\sin\theta\sin\phi & \cos\theta \end{pmatrix} \begin{pmatrix} a(\phi,\theta) \\ b(\phi,\theta) \\ c(\phi,\theta) \end{pmatrix} \quad (3)$$

Where $a(\phi,\theta), b(\phi,\theta), c(\phi,\theta)$ are the polarization functions for *x*, *y* and *z* components of the incident beam. In the case of commonly used TM and TE polarized cylindrical vector beam modes these functions have a simpler form independent of θ [1]. In this work we consider paraxial input field, purely transverse in nature for which $c(\phi,\theta)=0$ .The polarization matrix (Equ. (3)) can then be rewritten as

$$P(\theta,\phi) = \begin{pmatrix} a(\theta,\phi)(\cos\theta\cos^2\phi+\sin^2\phi)+b(\phi,\theta)(\cos\theta-1)\sin\phi\cos\phi \\ a(\cos\theta-1)\sin\phi\cos\phi+b(\phi,\theta)(\cos\theta\sin^2\phi+\cos^2\phi) \\ -a(\theta,\phi)\sin\theta\cos\phi-\sin\theta\sin\phi \end{pmatrix} = \begin{pmatrix} P_x(\theta,\phi) \\ P_y(\theta,\phi) \\ P_z(\theta,\phi) \end{pmatrix} \quad (4)$$

Now consider the generalized VV beam with Laguerre-Gauss (LG) beam distribution incident on the axicon. The polarization state of the generalized vector beam is

$$\begin{pmatrix} a(\phi,\theta) \\ b(\phi,\theta) \\ 0 \end{pmatrix} = \begin{pmatrix} \cos(m\phi+\delta) \\ \sin(m\phi+\delta) \\ 0 \end{pmatrix} \quad (5)$$

Where 'm' denotes the order of the vector beam and 'δ' is the phase difference between the constituent LG beams. The amplitude and phase distribution ($A(\rho_0,\phi)$) of the LG beam is [24].

$$A(\rho_0,\phi) = (\rho_0^2/w_0^2)^{\frac{|l|}{2}} L_p^{|l|}(2\rho_0^2/w_0^2)\exp(\frac{\rho_0^2}{w_0^2})\exp(il\phi)\exp(-ik\xi\rho_0) \quad (6)$$

Where $L_p^{|l|}$ is the generalized Laguerre polynomial and $\exp(-ik\xi\rho_0)$ is the axicon phase function defined as $\xi=(n-1)\tan\alpha$ (with 'n' the refractive index of the axicon material and 'α' the axicon open angle). Using this the electric field distribution at any point after the axicon when a generalized vector-vortex beam is focused by the axicon is written by substituting Equ.(2),(4),(5) and (6) in Equ.(1). The electric field components any point (ρ,β,z) is written as

$$E_x(\rho,\beta,z) = \frac{-iz\exp(ikr)}{\lambda r^2}\int_0^\infty d\rho_0 \int_0^{2\pi} d\phi P_x(\phi,\theta)(\rho_0^2/w_0^2)^{\frac{|l|}{2}} L_p^{|l|}(2\rho_0^2/w_0^2)\exp(\frac{\rho_0^2}{w_0^2}+il\phi-ik\xi\rho_0+ik\frac{\rho_0^2}{2r})$$
$$\exp[i\eta cos(\phi-\beta)]\rho_0 \quad (7a)$$

$$E_y(\rho,\beta,z) = \frac{-iz\exp(ikr)}{\lambda r^2}\int_0^\infty d\rho_0 \int_0^{2\pi} d\phi P_y(\phi,\theta)(\rho_0^2/w_0^2)^{\frac{|l|}{2}} L_p^{|l|}(2\rho_0^2/w_0^2)\exp(\frac{\rho_0^2}{w_0^2}+il\phi-ik\xi\rho_0+ik\frac{\rho_0^2}{2r})\times \quad \text{(7b)}$$

$$\exp[i\eta cos(\phi-\beta)]\rho_0$$

$$E_z(\rho,\beta,z) = \frac{-i\exp(ikr)}{\lambda r^2}\int_0^\infty d\rho_0 \int_0^{2\pi} d\phi[P_x(\phi,\theta)(\rho cos\beta-\rho_0\cos\phi)+P_y(\phi,\theta)(\rho\sin\beta-\rho_0\sin\phi)]\times$$

$$\text{(7c)}$$

$$(\rho_0^2/w_0^2)^{\frac{|l|}{2}} L_p^{|l|}(2\rho_0^2/w_0^2)\exp(\frac{\rho_0^2}{w_0^2}+il\phi-ik\xi\rho_0+ik\frac{\rho_0^2}{2r})\exp[i\eta cos(\phi-\beta)]\rho_0$$

Where $\eta = -k\rho\rho_0/r$.

The special cases for focusing of vector-vortex beams are realized by substituting the corresponding polarization matrix in the above Equ (7). The treatment presented above is valid for different types of focusing optical elements including lens and axicon and for different types of input optical beams, from plane wavefront scalar Gaussian beam to vector beam to generalized vector-vortex beam. However, as the objective of our work is to generate and understand sub-wavelength spot size focused beams with long Rayleigh range we restrict our treatment to axicon focusing of few special cases of VV beam, after verifying our results for lens focusing with already published work.

3. LENS FOCUSING OF VECTOR-VORTEX BEAMS

The focusing characteristics of cylindrical vector beam by high NA lenses and the focus shaping properties are well studied using Richads-Wolf diffraction integrals [2,3]. The mathematical formalism discussed in Section 2 is for the focusing of generalized VV beams by a conical lens, but as mentioned earlier it can be extended for lens focusing as well by incorporating the lens phase function instead of that of axicon. We used vectorial Rayleigh diffraction integral formalism to study the high NA focusing of vector-vortex beam, using the quadratic phase function for the lens: $\exp(-ik\rho_0^2/f)$, where 'f' is the focal length of the lens.

Now consider a monochromatic radially polarized beam of wavelength λ incident on the high-NA lens of focal length f. the electric field components in the focal region can be calculated by using Equ (7) after substituting z = (z-f), the corresponding polarization matrix for radial polarization and the lens phase function. The simulation results obtained for focusing of radially polarized beam field using our formalism are in good agreement with the previous results [2, 3]. Fig.2 shows the normalized intensity distribution near the focal region and the contribution of different electric field components towards total intensity, when a radially polarized beam is focused by a lens of NA=0.8.

3.1 Axicon Focusing of Azimuthally-polarized Vortex Beam

The polarization matrix for azimuthally polarized beam is obtained by substituting $\delta=\frac{\pi}{2}$ in Equ(5), and the polarization matrix (equ (4)) then becomes

$$P(\theta,\phi) = \begin{pmatrix} \sin m\phi \\ -\cos m\phi \\ 0 \end{pmatrix} \quad (8)$$
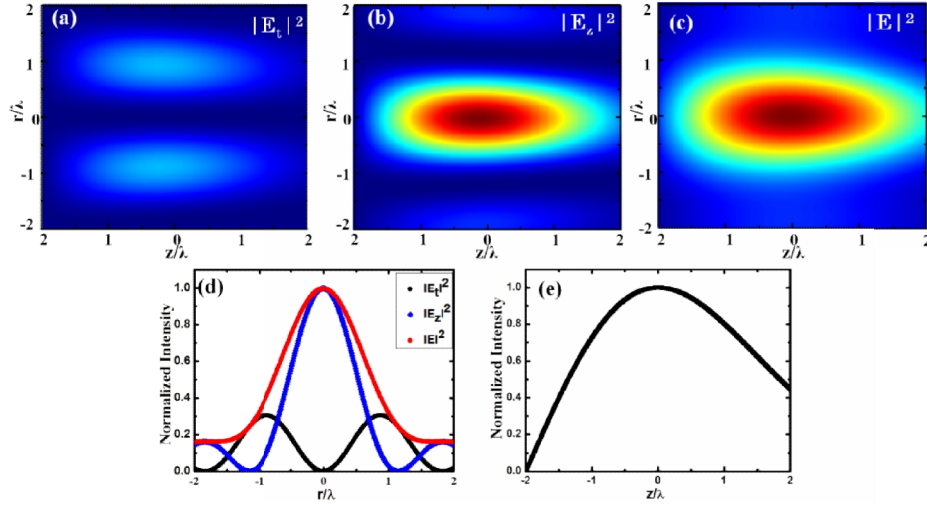

Fig. 2 (a),(b) and (c) are respectively the transverse and longitudinal field components and the total intensity with propagation; (d) shows the line profiles of the intensity distribution of (a) – (c) at the focal plane (Z=0); (e) shows the axial intensity with propagation distance

Substituting the polarization matrix elements in Equ (7) the field components at any position after the axicon can be written as

$$E_x(\rho,\beta,z) = \frac{-iz\exp(ikr)}{\lambda r^2}\int_0^R (\frac{\rho_0^{l+1}}{w_0^l})\exp(-\frac{\rho_0^2}{w_0^2})L_p^{|l|}(2\rho_0^2/w_0^2)\exp(-ik\xi\rho_0)\exp(ik\frac{\rho_0^2}{2r}) \times$$
$$[\pi(-i)i^{(l+m)}J_{(l+m)}(\eta)\exp[i(l+m)\beta + \pi ii^{(l-m)}J_{(l-m)}(\eta)\exp[i(l-m)\beta] \quad (9a)$$

$$E_y(\rho,\beta,z) = \frac{iz\exp(ikr)}{\lambda r^2}\int_0^R \frac{\rho_0^{l+1}}{w_0^l}\exp(-\frac{\rho_0^2}{w_0^2})L_p^{|l|}(2\rho_0^2/w_0^2)\exp(-ik\xi\rho_0)\exp(\frac{ik\rho_0^2}{2r}) \times$$
$$\{\pi i^{l+m}J_{l+m}(\eta)\exp[i(l+m)\beta] + \pi i^{(l-m)}J_{(l-m)}(\eta)\exp[i(l-m)\beta]\} \quad (9b)$$

$$E_z(\rho,\beta,z) = \frac{i\exp(ikr)}{\lambda r^2}\int_0^R (\frac{\rho_0^{l+1}}{w_0^l})\exp(-\frac{\rho_0^2}{w_0^2})L_p^{|l|}(2\rho_0^2/w_0^2)\exp(-ik\xi\rho_0)\exp(ik\frac{\rho_0^2}{2r}) \times$$
$$\{\rho\pi i^{l+m}(-i)J_{l+m}(\eta)\exp[i(l+m+1)\beta] + \rho\pi i^{l-1}(i)J_{l-m}(\eta)\exp[i(l+m-1)\beta]\}d\rho_0 \quad (9c)$$

We used an azimuthally polarized beam of order *m*=1 and helical charge *l*=+1 in our experiments under low NA focusing. The vector-vortex beam generator consists of a He-Ne laser (λ = 632.8 nm) and a 27.4 cm long two-mode optical fiber. The Gaussian beam from the He-Ne laser is passed through a polarizer-half wave plate combination to enable the

change of the plane of polarization of the linearly polarized input beam. This linearly polarized beam is coupled skew-off axially into the circular-core step-index two-mode optical fiber (V# = 3.805, length = 27.4 cm) using a 20x, 0.4 NA microscope objective lens, mounted on a 3-axis precision fiber launch system. The linear polarization of the input beam and the coupling angle are selected such that the output beam from the two-mode optical fiber is a cylindrical vector beam [25]. The output beam from the optical fiber is then collimated using 20x microscopic objective lens. Two cascaded half-wave plates are used after the collimated fiber output to rotate the spatial polarization state of the vector beam [1,3] which in turn passes through a spiral phase plate (VPP m-633 RPC Photonics, USA) and is subsequently focused by an axicon of open angle α=0.5°. The focused beam is then imaged using a CCD along the direction of propagation 'z'. The polarization characteristics of the focused beam are measured via spatially resolved Stokes polarimetry using a quarter-wave plate and polarizer combination [26]. The generated transverse field (longitudinal field E_z=0) is a superposition of orthogonal circularly polarized J_0 and J_2 Bessel functions as can be seen from Equs. (9). The beams described by the J_0 and J_2 Bessel functions have respectively a central maximum intensity and a vortex of topological charge $l = +2$ with intensity null at the centre. The on-axis superposition of the two beams with orthogonal circular polarization results in elliptically polarized field, leading to the formation of C-point and L-line in the beam cross-section [16, 17]. In the present case the *C*-point index defined as $I_c = \frac{1}{2\pi}\oint d\psi = \pm 1$,

where ψ is the polarization ellipse orientation, which rotates by 2π around the C-point. Fig.3 shows the theoretical simulations and the experimentally measured intensity distribution, polarization ellipse map and the ellipse orientation at the centre of the non-diffracting range Z=Z_{max}/2, where $Z_{max} = \omega_0 (k/k_r)$ with $k_r \approx (n-1)\alpha k$, k=2π/λ is the wave vector.
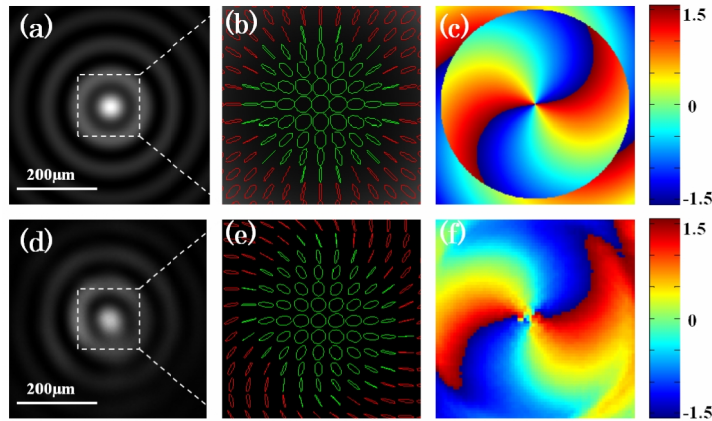

Fig. 3 (a)-(c) are respectively the theoretical simulations of intensity distribution, polarization ellipse map and the polarization ellipse orientation. (d)-(f) are the corresponding experimental results, all are at Z = Zmax/2

The polarization ellipse orientation around the *C*-point depends on the phase difference between the constituent J_0 and J_2 beams. The radial type variation in the polarization ellipse orientation around the *C*-point in Fig. 3 is due to the Gouy phase difference of 2π between the constituent beams with an additional Gouy phase of π added when the beams pass through the first focus [27].

With the simulation results (using Equ. 9) matching the experimental results we proceed to simulate the condition when the azimuthally-polarized vector-vortex beam is focused by a high NA axicon. The focusing element is an axicon of open angle α=70° and the input beam is an azimuthally polarized vortex beam of helical charge *l*=+1 having a waist width ω_0=5mm with λ=632.8nm. Fig.4 shows the propagation of the electric field components in the focal region calculated using Equ. (9). From the figure it is seen that when an azimuthally polarized vortex beam is focused by high-NA axicon the longitudinal component of the field goes to zero resulting in a purely transverse focal field.
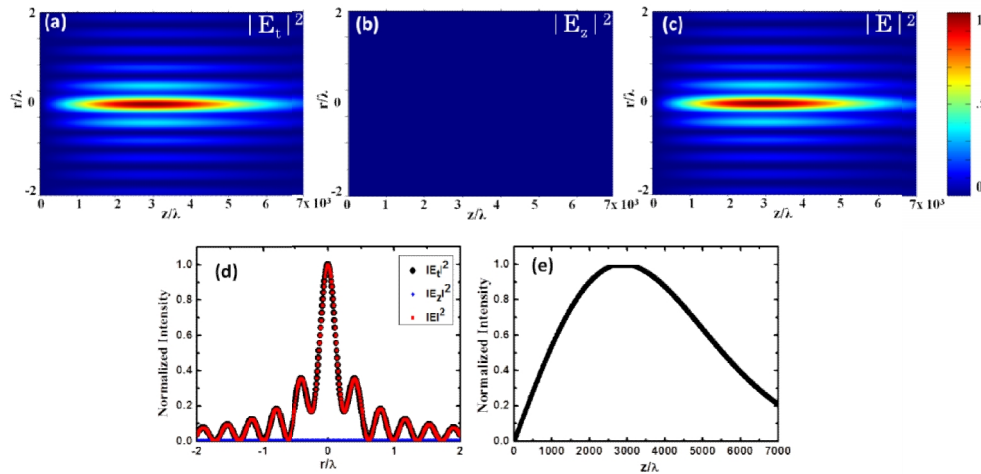

Fig. 4 (a),(b) and (c) are respectively the transverse and longitudinal field components and the total intensity with propagation; (d) shows the line profiles of the intensity distribution of (a) – (c) at Z=Zmax/2; (e) shows the axial intensity with propagation distance

It is also important to note here that the diameter of the central spot is calculated to be 0.43λ at $Z=Z_{max}/2$ and it propagates without diverging for a long distance of (80λ) as compared to the size of the input beam and such beams are known as optical needle beam [5]. Alternate optical needle beam generation methods include focusing of phase modulated radially polarized beam by high NA lens [5], high NA lens axicon [28], focusing of radially polarized Bessel-Gauss (BG) beam [29] and reversing electric dipole array radiation [30] but all with much smaller non-diverging range that our results presented here. These long range optical needle beams find applications in polarization sensitive orientation imaging [31,32], and light-matter interaction in the nano-scale [33]. Longitudinally polarized optical needle beams are also useful in particle manipulation and acceleration [34,35]. It is important to note here that all these above-mentioned methods for the generation of optical needle beams [5,28-30] involve use of either complex phase modulation or amplitude modulation of the input beam. The high NA axicon based method presented here is simpler and involves direct axicon focusing of vector-vortex beam.

3.2 Axicon Focusing of Radially-polarized Vortex Beam

Next, we extend our formalism to generate longitudinally polarized optical needle beam by focusing radially polarized vortex beam using an axicon. The polarization matrix for radial

polarization is obtained by substituting $\delta = 0$ in Equ. (5) for which the polarization matrix (Equ. 4) is written as:

$$P(\theta, \phi) = \begin{pmatrix} \cos\theta\cos m\phi \\ \cos\theta\sin m\phi \\ \sin\theta \end{pmatrix} \tag{10}$$

The electric field components after the axicon at any position along the propagation direction 'Z' is obtained by substituting the polarization elements in Eqn.(7) and we get

$$E_x(\rho,\beta,z) = \frac{-iz\exp(ikr)\cos(\theta)(\pi)}{\lambda r^2}\int_0^R (\frac{2\rho_0^{2|l|+1}}{w_0^{2|l|}})\exp(-\frac{\rho_0^2}{w_0^2})L_p^{|l|}(2\rho_0^2/w_0^2)\exp(-ik\xi\rho_0)\exp(ik\frac{\rho_0^2}{2r})\times \tag{11a}$$

$$[\pi i^{l+m}J_{l+m}(\eta)\exp(i(l+m)\beta) + \pi i^{l-m}J_{l-m}(\eta).\exp(i(l-m)\beta]d\rho_0$$

$$E_y(\rho,\beta,z) = \frac{-iz\exp(ikr)\cos(\theta)}{\lambda r^2}\int_0^R (\frac{\rho_0^{l+1}}{w_0^l})\exp(-\frac{\rho_0^2}{w_0^2})L_p^{|l|}(2\rho_0^2/w_0^2)\exp(-ik\xi\rho_0)\exp(ik\frac{\rho_0^2}{2r})\times \tag{11b}$$

$$[\pi i^{l+m}(-i)J_{l+m}(\eta)\exp[i(l+m)\beta] + \pi i^{l-m}(i)J_{l-m}(\eta)\exp[i(l-m)\beta]d\rho_0$$

$$E_z(\rho,\beta,z) = \frac{i\exp(ikr)\cos\theta\exp(il\beta)}{\lambda r^2}\int_0^R (\frac{\rho_0^{l+1}}{w_0^l})\exp(-\frac{\rho_0^2}{w_0^2})L_p^{|l|}(2\rho_0^2/w_0^2)\exp(-ik\xi\rho_0)\exp(ik\frac{\rho_0^2}{2r})\times \tag{11c}$$

$$[\rho\pi i^{l+m}J_{l+m}(\eta) + \rho\pi i^{l-m}J_{l-m}(\eta) - \rho_0 2\pi i^l J_l(\eta)]d\rho_0$$

In our experiment the spirally polarized vector beam output from the generator is made radial by rotating the two half-wave plate orientation which is then passed through the SPP and is subsequently focused using the axicon of α=0.5º corresponding to the case with *m=+1, l=+1*. Here the paraxial focus of the axicon ensures that the contribution of the longitudinal component of electric field to the total intensity is negligibly small. As before the focused beam is imaged using the CCD camera and its polarization characteristics are obtained by measuring the Stokes parameters. Fig.5 shows the theoretical simulation and experimentally measured intensity distribution, polarization ellipse map and its orientation in the middle of the non-diverging region (Z=Z$_{max}$/2).
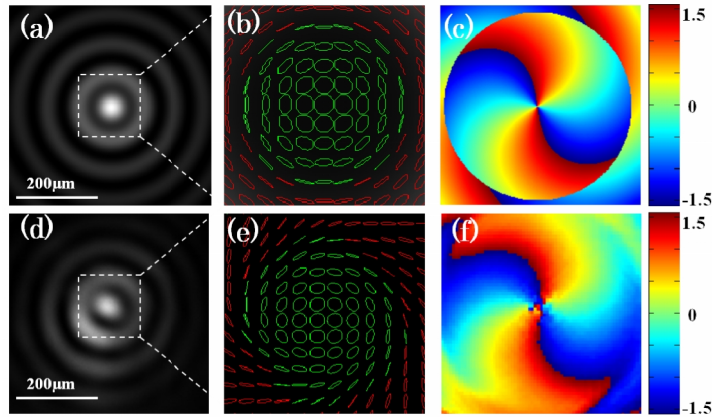
Fig. 5 (a)-(c) are respectively the theoretical simulations of intensity distribution, polarization ellipse map and the polarization ellipse orientation. (d)-(f) are respectively the corresponding experimental results, all are at Z=Zmax/2

Focusing radially-polarized beam of order m=1 results in a central bright spot for *l*=0, 1 [36], which for the *l*=+1 case is transversely polarized. To generate longitudinally polarized optical needle beam we choose radially polarized vortex beam and focus it using a high NA axicon. The electric field components can be calculated from Equ. (11). If we choose an axicon with an open angle of α=70º the resulting longitudinally polarized central bright spot intensity is much more than the transverse component. For radially polarized vortex beam, with *l*=+1 and beam width 5mm input to the axicon Fig.6 shows the theoretically simulated propagation characteristics. The spot size of the central bright spot is calculated to be 0.48λ and is propagating without divergence for up to a distance of 80λ.
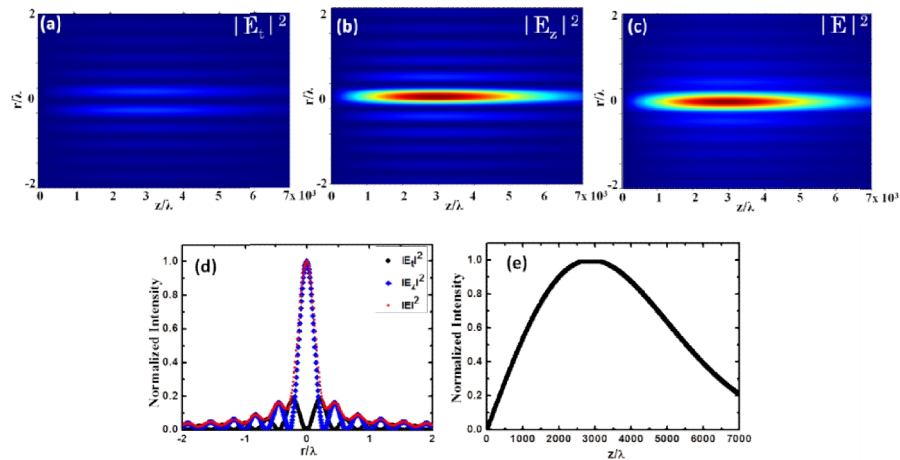

Fig. 6 (a), (b) and (c) respectively are the transverse and longitudinal components and total intensity distribution with propagation; (d) shows the line profiles of the intensity distribution of (a) – (c) at Z=Zmax/2; (e) shows the axial intensity with propagation distance

Using the mathematical formalism developed here based on vectorial Rayleigh diffraction integrals the focusing characteristics of vector-vortex beam by an axicon is studied. The focusing of VV beam leads to the formation of polarization singularities depending on the order of the vector beam and the helical charge. It is shown that for an azimuthally polarized vortex beam the focusing leads to the formation of *C*-point singularity with index 1. The *C*-point of index 1 is formed by the superposition of J_0 and J_2 Bessel beams which are formed by adding and subtracting helical charges of the constituent beams of the cylindrical vector beam. Axicon focusing ensures longer non-diverging range where the axial phase of the beam is stationary. This ensures the polarization singular pattern free from phase distortions due to propagation. Direct generation of higher order phase vortex leads to the splitting of the helical charges but this splitting is minimum in our method. Higher-order *C*-points can be generated by changing the order (*m*) of the vector beam and by suitably adjusting the helical charge (*l*) of the vortex beam. For example *C*-point of index 2 can be generated by focusing a vector beam of order *m*=2 carrying a helical charge *l*= +2. The sign of the C-point index can also be changed by changing the handedness of the superposing Bessel beams which can be achieved by including a half wave plate after the axicon. Also, the optical needle beams generated by high NA axicon focusing of vector-vortex beams has a non-diverging range which is one order of magnitude higher than achieved by other methods.

4. CONCLUSION

A general mathematical formalism is developed for the calculation of electric field components based on vectorial Rayleigh integrals, for VV beams focused by an axicon. The formation of polarization singularities by focusing VV beam by the axicon is studied theoretically and experiments were performed to validate the theoretical predictions under low NA focus conditions. The *C*-point of index 1 with different polarization ellipse structures were generated experimentally by low NA focusing of azimuthal and radial polarized VV beams. The formalism is extended to high NA axicon focusing of VV beams resulting in the generation of purely transverse or purely longitudinally polarized optical needle beams. It is shown using theoretical simulations that our method can generate optical needle beam of spot-size (0.43λ) with long non-diverging range of 80λ.

ACKNOWLEDGEMENTS

COMPETING INTERESTS

Authors have declared that no competing interests exist.

REFERENCES

1. Qiwen Zhan. Cylindrical vector beams: from mathematical concepts to applications. Advances in Optics and Photonics. 2009;1:1–57.
2. Youngworth KS, Brown TG. Focusing of high numerical aperture cylindrical vector beams. Opt. Exp. 2000;7:77–87.
3. Qiwen Zhan, James Leger Focus shaping using cylindrical vector beams Opt. Exp. 2002;10:324-331.

4.   Dorn R, Quabis S, Leuchs G. Sharper focus for a radially polarized light beam. Phys. Rev. Lett. 2003;91:233901.

5.   Haifeng Wang, Luping Shi, Boris Luk`yanchuk1, Colin Sheppard, Chong Tow Chong. Creation of a needle of longitudinally polarized light in vacuum using binary optics. Nature Photonics. 2008;2:501.

6.   GH Yuan, SB Wei, X.-C. Yuan. Non diffracting transversally polarized beam. Opt. Lett. 2011;36:3479-3481.

7.   Willing KI, Rizzoli SO, Westphal V, Jahn R, Hell SW, STED-microscopy reveals that synaptotagmin remains clustered after synaptic vesicle exocytosis. Nature. 2006;440:935.

8.   Romea RD, Kimura WD. Modeling of inverse Čerenkov laser acceleration with axicon laser-beam focusing. Phys. Rev. D.1990;42:1807.

9.   Lu Huang, Honglian Guo, Jiafang Li, Lin Ling, Baohua Feng, Zhi-Yuan Li. Optical trapping of gold nanoparticles by cylindrical vector beam. Opt. Lett. 2012;37:1694-1696.

10. Liangxin Yang, Xiangsheng Xie, Sicong Wang, Jianying Zhou. Minimized spot of annular radially polarized focusing beam. Opt. Lett. 2013;38:1331-1333.

11. Yuan GH, Wei SB, X.-C. Yuan. Non-diffracting transversally polarized beam. Opt. Lett 2011;36:3479-3481.

12. Dowski ER, Jr., Cathey WT. Extended depth of field through wave-front coding. Appl. Opt. 1995;34(11):1859–1866.

13. Botcherby EJ, Juškaitis R, Wilson T. Scanning two photon fluorescence microscopy with extended depth of field. Opt. Commun. 2006;268(2):253–260.

14. Kazuhiro Sasaki, Kazuhiro Kurokawa, Shuichi Makita, Yoshiaki Yasuno. Extended depth of focus adaptive optics spectral domain optical coherence tomography. Opt. Exp. 2012;3:2353-2370.

15. Dufour P, Piché M, Koninck Y De, McCarthy N. Two-photon excitation fluorescence microscopy with a high depth of field using an axicon. Appl. Opt. 2006;45(36):9246–9252.

16. Isaac Freund. Polarization singularity indices in Gaussian laser beams. Opt. Commun. 2002;201:251–270.

17. Florian Flossmann, Kevin O'Holleran, Mark R. Dennis, Miles J. Padgett. Polarization Singularities in 2D and 3D Speckle Fields. Phys. Rev. Lett. 2008;100:203902(1–4).

18. Zhang W , Liu S, Li P, Jiao X, Zhao J. Controlling the polarization singularities of the focused azimuthally polarized beams. Opt. Exp. 2013;21:974–983.

19. Schoonover RW, Visser TD. Polarization singularities of focused, radially polarized fields. Opt. Exp. 2006;14(12):5733–5745.

20. Ciattoni A, Crosignani B, Porto PD. Vectorial analytical description of propagation of a highly nonparaxial beam. Opt. Commun. 2002;202:17–20.

21. Luneburg RK, Mathematical Theory of Optics (University of California Press, Berkeley; 1966.

22. Yaoju Zhang, Ling Wang, Chongwei Zheng. Vector propagation of radially polarized Gaussian beams diffracted by an axicon. J. Opt. Soc. Am. A. 2005;22:2542-2546.

23. Khonina SN, Kazanskiy NL, Volotovsky SG. Influence of Vortex Transmission Phase Function on Intensity Distribution in the Focal Area of High-Aperture Focusing System. Optical Memory and Neural Networks (Information Optics). 2011;20:23–42.

24. Arlt J, Dholakia K. Generation of high-order Bessel beams by use of an axicon. Opt. Commun. 2000;177:297.

25. Nirmal K. Viswanathan, VV. Inavalli. Generation of optical vector beams using a two-mode fiber. Opt. Lett. 2009;34:1189-1191.

26. Goldstein DH, Collett E, Polarized Light, 2nd ed. Marcel Dekker; 2003.

27. Philip GM, Vijay Kumar, Giovanni Milione, Viswanathan NK. Manifestation of the Gouy phase in vector-vortex beams. Opt. Lett. 2012;37:2667-2669.

28. Suresh P, Mariyal C, Rajesh KB, Pillai TV, Jaroszewicz Z. Generation of a strong uniform transversely polarized nondiffracting beam using a high-numerical-aperture lens axicon with a binary phase mask. Appl Opt. 2013;52(4):849-853.

29. Yikun Zha, JingsongWei, Haifeng Wang, Fuxi Gan. Creation of an ultra-long depth of focus super-resolution longitudinally polarized beam with a ternary optical element. J. Opt. 2013;15:075703.

30. Jiming Wang, Weibin Chen, Qiwen Zhan. Engineering of high purity ultra-long optical needle field through reversing the electric dipole array radiation. Opt. Expr. 2010;18:21965–21972.

31. Abouraddy AF, Toussaint KC, Jr. Three-dimensional polarization control in microscopy. Phys. Rev. Lett. 2006;96(15):153901.

32. Novotny L, Beversluis MR, Youngworth KS. Brown TG. Longitudinal field modes probed by single molecules. Phys. Rev. Lett. 2001;86(23):5251–5254.

33. Banzer P, Peschel U, Quabis S, Leuchs G. On the experimental investigation of the electric and magnetic response of a single nano-structure. Opt. Exp. 2010;18(10):10905–10923.

34. Takeuchi S, Sugihara R, Shimoda K. Electron acceleration by longitudinal electric field of a Gaussian laser beam. J. Phys. Soc. Jpn. 1994;63(3):1186–1193.

35. Friese MEJ, Nieminen TA, Heckenberg NR, Rubinsztein-Dunlop H. Optical alignment and spinning of laser-trapped microscopic particles. Nature. 1998;394(6691):348–350.

36. Helseth LE. Optical vortices in focal regions. Opt. Commun. 2004;229:85-91.